



PAPER • OPEN ACCESS

Advanced damping solutions for single-particle impact dampers: exploring design parameters with a linear contact approach

To cite this article: Muhammad Ayaz Akbar and Hassan Raza 2025 Eng. Res. Express 7 035503

View the article online for updates and enhancements.

You may also like

- Peltier coefficient measurement in a thermoelectric module Javier Garrido, Alejandro Casanovas and José María Chimeno
- Mechanical and electronic properties of Janus monolayer transition metal dichalcogenides
 Wenwu Shi and Zhiguo Wang
- Two-dimensional intrinsic ferromagnetic materials of Janus 2H-NbXY (X, Y = S, Se and Te, X Y) monolayers with high Curie temperature and large magnetic anisotropy

Tianxing Wang, Tian Tian, Mengxin Li et

Engineering Research Express



OPEN ACCESS

RECEIVED

3 April 2025

REVISED

16 June 2025

ACCEPTED FOR PUBLICATION

25 June 2025

PUBLISHED

2 July 2025

Original content from this work may be used under the terms of the Creative Commons Attribution 4.0 licence.

Any further distribution of this work must maintain attribution to the author(s) and the title of the work, journal citation and DOI.



PAPER

Advanced damping solutions for single-particle impact dampers: exploring design parameters with a linear contact approach

Muhammad Ayaz Akbar¹ and Hassan Raza^{2,*}

- ¹ Institute of Advanced Interdisciplinary Research and Technology, Shenzhen MSU-BIT University, Shenzhen 518172, People's Republic of China
- Department of Mechanical Engineering, The Hong Kong Polytechnic University, Hong Kong SAR, People's Republic of China
- * Author to whom any correspondence should be addressed.

E-mail: hraza@polyu.edu.hk

Keywords: single-particle impact damper, passive vibration control, tuned mass damper, damping performance, 3D printing

Abstract

Single-particle impact dampers (SPIDs) are passive vibration absorbers (PVAs) that enclose a free-moving particle (mass) within a host structural cavity. SPIDs are easier to develop and install than known PVAs, but their nonlinearities complicate parameter selection. Using a linear contact model (LCM), this study identifies additional design parameters to enhance damping. A numerical model of a SPID on a SDOF structure is employed using the LCM to mimic particle-structure interactions. SPID demonstrates exceptional damping performance (amplitude ratio $X/Y \le 10$) throughout a wide variety of design parameters, including dimensionless clearance magnitudes (D = 5–20) and damping ratios (ζ _eq = 0.07–0.45). This differs significantly from traditional tuned mass dampers (TMD), which require a restricted ideal parameter range (e.g., ζ _opt = 0.15 for μ = 0.1) to prevent detuning. For experimental validation, four 3D-printed materials (B10, B15, B20, and B50) with varied stiffness (k = 6.35–48.08 kN m $^{-1}$) and damping coefficients (c = 5.62–23.88 Ns m $^{-1}$) are evaluated. SPID lowers resonant amplitudes by up to 57% (e.g., B50 at D \approx 7.5: simulated X/Y = 8.34 versus experimental X/Y = 9.68), demonstrating the correctness of the numerical model (error: <15%). This study shows that SPID is effective when reducing resonant peaks and simplicity matters more than optimal attenuation.

1. Introduction

A single-particle impact damper (SPID) is a passive vibration absorber where a single-mass, referred to as particle is placed inside a cavity or container on the host structure. The particle can move freely inside the cavity or container. The particle moves with the vibration of the host structure under any external force and collides with the walls of the cavity or container. The working principle of a SPID is to suppress vibration energy through momentum exchange and energy dissipation with collisions between the primary structure and particles (Friend and Kinra 2000, Wong et al 2009, Song et al 2024). SPIDs have demonstrated significant potential across various engineering applications (Gardonio and Elliott 2000, Chen and Georgakis 2013, Gourc et al 2015, Chan et al 2016, Duvigneau et al 2016, Hu et al 2016, Jadhav and Awasare 2016, Veeramuthuvel et al 2016) such as structural vibration control, machinery, aerospace, etc However, engineers seek greater confidence in employing them for delicate engineering tasks due to their nonlinear behavior and the need of more analytical understanding (Liu et al 2002, Wong and Rongong 2009, Afsharfard and Farshidianfar 2011, Sánchez and Manuel Carlevaro 2013). The effectiveness of SPID performance depends on various factors, such as the damper's configuration, particle properties, and the collision's characteristics. Engineers have made efforts and evaluated a number of methods to increase the effectiveness of SPID in real engineering problems (Ekwaro-Osire and Desen 2016, Li and Darby 2016, Papalou and Masri 2016, Yang and Wang 2019, Jin et al 2024, Zhou et al 2025). In the absence of analytical models, the researchers used experimental and numerical models to establish the design procedures for single-particle impact dampers (Fadel Miguel et al 2016, Snoun and

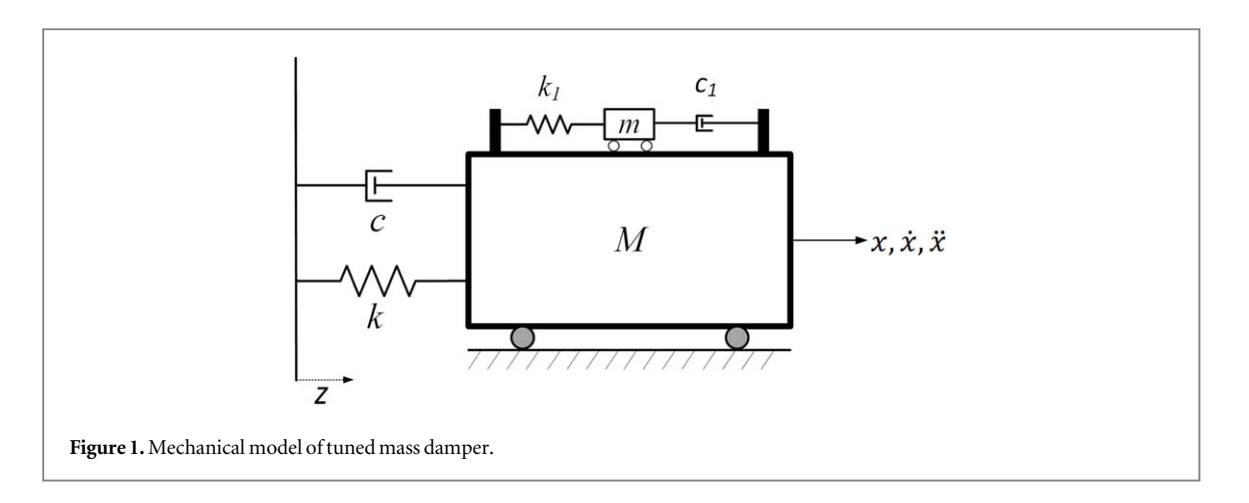
Trigui 2018, Chen et al 2019, Huang et al 2021). It is determined that the clearance magnitude and mass ratio are the fundamental design parameters for SPID (Gagnon et al 2019). Some studies have tried formulating a strategy for determining a SPID's optimal clearance magnitude and mass ratio (Popplewell and Liao 1991, Bryce et al 2001, Michael et al 2004, Xu et al 2004). There have been studies on enhancing the performance of SPID, trying to find the optimal clearance, while a few studies considered particle shape as well (Marhadi and Kinra 2005, Sánchez et al 2013).

Particle damping has garnered significant attention in recent years due to its simplicity and effectiveness in vibration mitigation. Traditional particle damper designs often rely on metallic or hard materials for their particles, which offer high stiffness and predictable behavior (Akbar et al 2024a, 2024b). However, advancements in material science and computational techniques have opened new avenues for optimizing particle dampers (Prasad et al 2022). For instance, recent studies have explored the use of multimodal particle configurations to enhance energy dissipation (Badri et al 2021, Jin et al 2021, Lu et al 2021). A recent study presented a design of particle damper for simultaneously achieving dynamic balance and reducing mechanical vibrations in motor reducers (Tran et al 2025). In another study, researchers investigated the applications of particle dampers in gearbox vibration suppression experimentally (Patil et al 2025). Song et al analyzed the vibration reduction performance of a vibration isolation system based on particle damping (Song et al 2024). Additionally, the integration of damping layers within the particle cavity has shown promise in improving broadband vibration suppression (Li et al 2019, Zhao et al 2019). Computational advances, such as machine learning-based optimization, have also enabled rapid design parameter exploration, potentially surpassing traditional trial-and-error methods (Guo et al 2024, Kumar and Kumar 2024, Guo et al 2025). These developments highlight the evolving landscape of particle damping and its potential for broader applications beyond traditional engineering systems.

After reviewing existing methods aimed at enhancing the performance of SPID, it is found that nature of impact has a significant role in overall damping performance. The nature of the impact surface stands as a critical parameter in the design of SPID and holds potential for significantly improving damping efficacy. While some studies have delved into investigating the impact surface through the utilization of the coefficient of restitution (Masri 1970, Wang and Dan 2022, Prasad *et al* 2023), it is usually fixed to a particular value in the simulations. On the other hand, the impact surface has been studied experimentally by altering the particle material to change the coefficient of restitution between the particle and primary mass (Hastie 2013). The particle material can change the impact characteristics but poses the challenge of maintaining mass ratio as the softer material tends to have a lighter mass. Previous investigations have concluded that metallic particles outperform their softer counterparts (Prasad *et al* 2022).

Drawing from existing literature, it is imperative to analyze the influence of collision characteristics on both damping performance and the optimization of SPID. The literature underscores the utilization of the coefficient of restitution to represent collision nature. A lower coefficient of restitution signifies substantial energy dissipation coupled with reduced momentum transfer, whereas a higher coefficient indicates less energy dissipation but greater momentum transfer. Achieving an optimal balance between momentum transfer and energy dissipation is essential for bolstering damping efficacy (Akbar et al 2023). Employing the coefficient of restitution to characterize collisions requires certain assumptions, such as neglecting impact duration and assuming robust impacts. These assumptions are inadequate to replicate the collision which is not fully elastic and includes soft materials (Akbar et al 2024a, 2024b). Hence, this article employs a linear contact model to represent collision characteristics. The linear contact model employs a combination of a linear spring and a damper dashpot to simulate stiffness and energy dissipation during non-elastic collisions. While collision phenomena are inherently complex and nonlinear in practice, a linear equivalent model can capture the fundamental physics of a collision and streamline numerical analysis. In addition, experimental validation is conducted to validate the results obtained from numerical analysis. The primary objective of the study is to demonstrate that SPID exhibits notable performance in attenuating resonance peaks across a broader spectrum of design parameters, presenting a viable alternative to tuned mass dampers for such applications. To validate the conclusions drawn from numerical analysis, several cushioning materials with varying mechanical properties (including stiffness and damping coefficient) are fabricated via 3D printing. These materials are then integrated into SPID and evaluated on a SDOF structure subjected to harmonic ground motions.

Moreover, TMD typically offers superior damping compared to SPID, the practical complexities associated with their design and installation can be excessively complicated in practice. TMD has well-established analytical models and optimal design methodologies, positioning them as a theoretical benchmark in passive vibration absorption. However, their effectiveness hinges on precise design parameters such as stiffness and damping coefficients, rendering the finding of materials with the specific properties both challenging and costly. In addition, variations in the mechanical properties (including stiffness and internal damping) of the primary structure may necessitate additional tuning of the TMD for optimal performance. Given the limited range of design parameters and the challenging design and installation, SPID find effectiveness in applications where



minimizing vibration amplitude isn't the primary concern, and the damper's role is primarily to mitigate resonance peaks and safeguard the host structure from excessive amplitudes at resonance.

Considering the complexity of TMD design, this study provides a design methodology of SPID with linear contact model. The linear contact model, despite its simplicity, incorporates the fundamental properties of impact such as impact duration and force. The numerical model is validated with experimental results, and it is proven that the linear contact model can be successfully used in impact damper models. The result from numerical model concludes that the SPID can be designed with a several design combinations without compromising on damping performance which verifies the straightforward design procedure of SPID. The experimental and numerical findings presented in this study demonstrate that SPID not only diminish resonance peaks but also substantially reduce vibration amplitudes at resonance, highlighting the effectiveness of SPID with their comparatively simpler design and installation methods at a lower cost.

The remainder of this paper is structured as follows: section 2 explains the theoretical analysis, detailing the analytical and numerical models of a TMD and the proposed SPID. Section 3 illustrates the findings and discussions derived from the theoretical analysis, along with key conclusions drawn. In section 4, experimental validations of the numerical results are presented. Finally, section 5 summarizes the significant conclusions drawn from this study.

2. Theoretical analysis

2.1. Tuned mass damper (TMD)

TMD stands as a conventional dynamic vibration absorber, which is well-known with established analytical models for optimal design (Zilletti *et al* 2012, Wong 2016). Mechanical model of a TMD is shown in figure 1. TMD can effectively suppress vibrations when design parameters are precisely selected employing established methodologies. The optimal parameter range is exceedingly narrow, making precise parameter determination challenging in practical applications, particularly the damping coefficient (Yang *et al* 2021). The selection of design parameters outside the optimal range may lead to detuning issues in TMD. Moreover, a TMD generally needs to be tuned for the natural frequency of the structure, limiting their effectiveness to specific frequencies (Zhang *et al* 2022). The dynamic response of the SDOF structure with a TMD relative to ground motion amplitude can be described as follows (Wong *et al* 2018),

$$\frac{X}{Y} = \sqrt{\frac{(\gamma_a^2 - \lambda^2)^2 + (2\gamma_a \lambda \zeta_a)^2}{[(1 - \lambda^2)(\gamma_a^2 - \lambda^2) - \mu \gamma_a^2 \lambda^2]^2 + [2\gamma_a \lambda \zeta_a (1 - \lambda^2 - \mu \lambda^2)]^2}}$$
(1)

where $\mu = m/M$, ω_a is the natural frequency of the absorber, $\gamma_a = \omega_a/\omega_n$ is the frequency ratio between the primary mass and TMD, $\lambda = \omega/\omega_n$ is the frequency ratio between the excitation frequency and the natural frequency of primary mass. The optimal design criteria for the TMD were established by Den Hartog (Hartog 1956) as,

$$\gamma_{opt} = \frac{1}{1+\mu} \tag{2}$$

$$\zeta_{opt} = \sqrt{\frac{3\mu}{8(1+\mu)}}\tag{3}$$

The optimal natural frequency and optimal damping ratio are depending upon the mass ratio (μ).

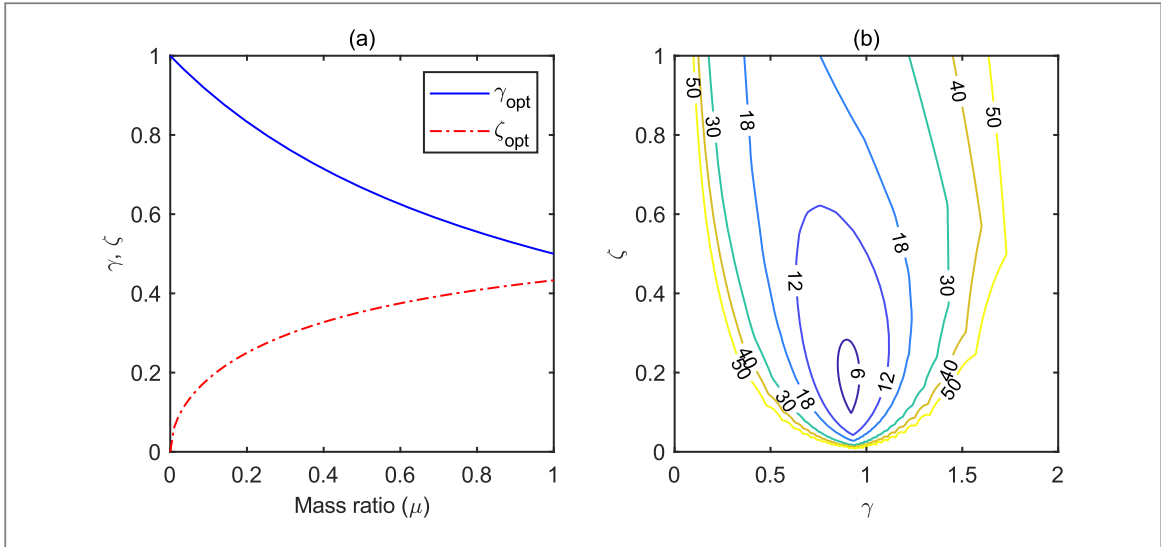


Figure 2. (a) Optimal design parameters of TMD with respect to mass ratio (μ); (b) Maximum dynamic vibration amplitude of host structure with various design combinations at $\mu=0.1$.

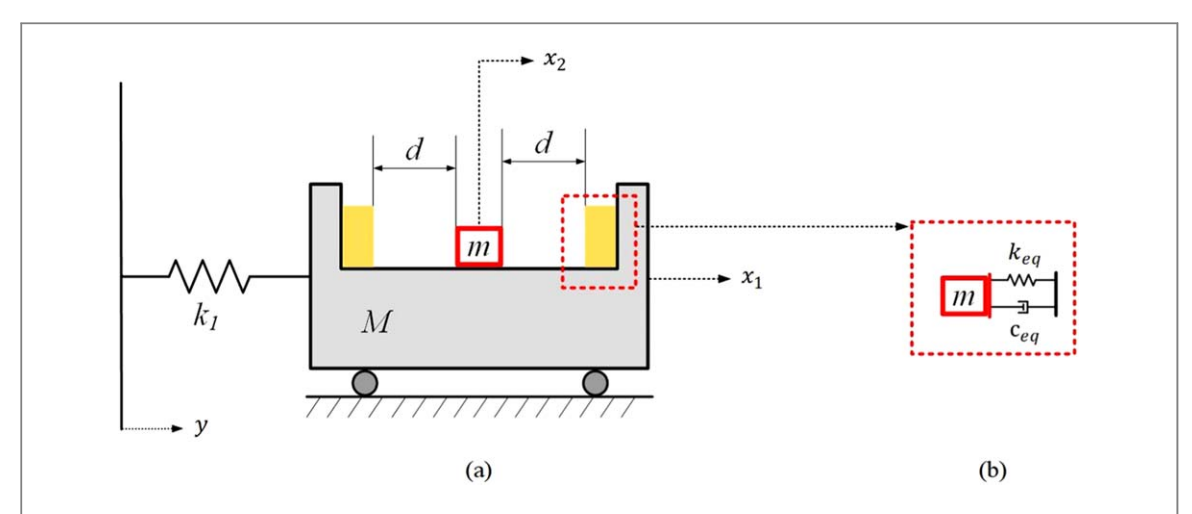


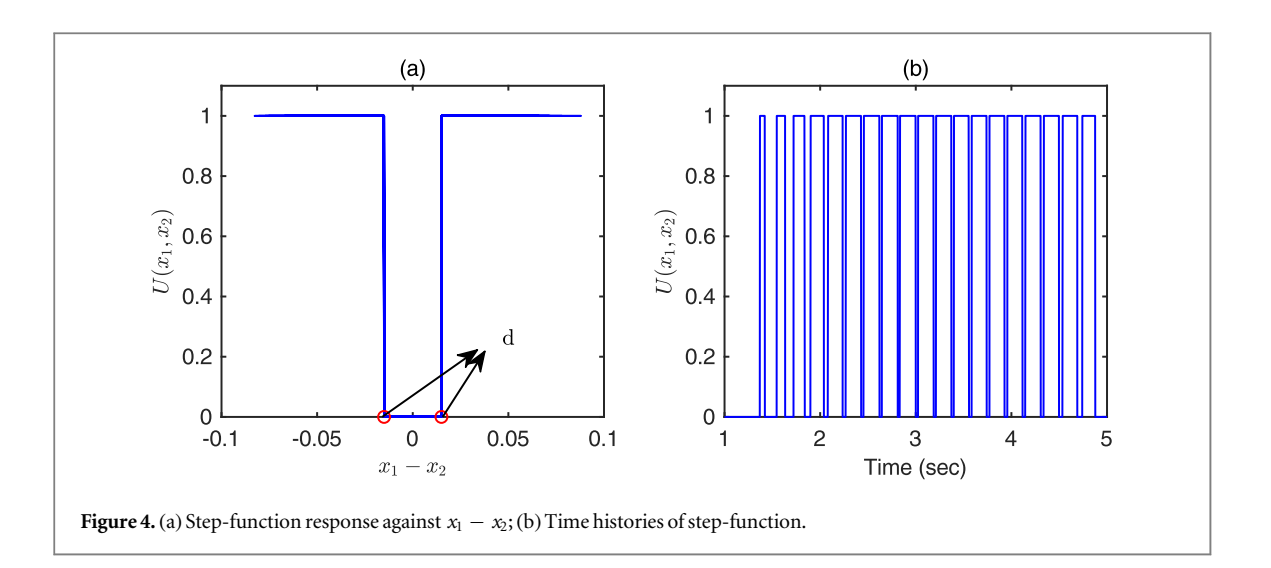
Figure 3. (a) Mechanical model of single-particle impact damper attached to an SDOF structure; (b) Equivalent modelling of soft impact surface when in contact with moving mass.

Figure 2(a) illustrates how design parameters such as the optimal frequency ratio γ_{opt} and damping ratio ζ_{opt} , evolve in relation to the mass ratio. However, increasing the mass of the absorber for vibration control is typically constrained by numerous factors. Hence, a mass ratio of 10% additional mass $\mu=0.1$ is employed, falling within an acceptable range. Figure 2(b) portrays the dynamic response variation of the host structure under different design parameters when $\mu=0.1$. It is evident from the graph that TMD parameters must remain fixed at specific levels to achieve optimal damping; even slight alterations in design parameters could lead to a significant reduction in damping effectiveness.

2.2. SPID with a linear contact model

SPID includes a single mass referred to as particle placed within a cavity or container on the host structure. The particle has the freedom to move within the cavity or container, following the direction of vibration of the host structure. Figure 3(a) illustrates a mechanical model of a SPID integrated with a SDOF structure. The particle collides with the host structure when the relative motion between them equals the clearance distance, denoted as 'a'. This collision can be represented using a linear contact model, as illustrated in figure 3(b). The duration and dynamics of the collision depends upon the mechanical properties of the materials involved. For instance, if the collision surface is rigid, the collision will be robust, whereas softer surface will result in an extended duration of impact.

The SPID model introduces an additional design parameter, namely clearance, compared to the TMD. When the particle is not in contact with the impact surface, the equations of motion for the primary mass and particle, with no friction between them, can be expressed as,



$$(M+m)\ddot{x}_1 + k_1(x_1 - y) = 0 (4)$$

$$m\ddot{\mathbf{x}}_2 = 0 \tag{5}$$

However, once the particle and primary mass come into contact, the equations of motion become,

$$M\ddot{x}_1 + k_1(x_1 - y) + k_{eq}H(x_1, x_2) + c_{eq}G(\dot{x}_1, \dot{x}_2) = 0$$
(6)

$$m\ddot{x}_2 - k_{eq}H(x_1, x_2) - c_{eq}G(\dot{x}_1, \dot{x}_2) = 0$$
(7)

Here $H(x_1, x_2)$ and $G(\dot{x_1}, \dot{x_2})$ are the nonlinear impact functions defined as,

$$H(x_1, x_2) = (x_1 - x_2 - d)U(x_1, x_2) + (x_1 - x_2 + d)U(x_1, x_2)$$
(8)

$$G(\dot{x}_1, \dot{x}_2) = (\dot{x}_1 - \dot{x}_2)u(x_1 - x_2 - d) + (\dot{x}_1 - \dot{x}_2)u(-x_1 + x_2 - d)$$
(9)

Here $U(x_1, x_2)$ is the unit step function known as the 'Heaviside' function in MATLAB software. The output of this function is 0 or 1 based on x_1 and x_2 and the clearance magnitude d. It is defined as,

$$U(x_1, x_2) = \begin{cases} 1, & \text{if } x_1 - x_2 = d \text{ or } -x_1 + x_2 = d \\ 0, & \text{if Elsewhere} \end{cases}$$
 (10)

This step function discerns impacts occurring on either side of the cavity, resulting in an output value of 1, as illustrated in figure 4. In figure 4(a), the step function is graphed alongside the relative motion of both masses, with the distance between them denoted by a red circle. Whenever the relative distance between the masses equals or exceeds the clearance on either side, the impulse response function records a value of 1, indicating impact detection in the analysis. Figure 4(b) displays the time response of the impulse response function.

The nonlinear functions $H(x_1, x_2)$ and $G(\dot{x_1}, \dot{x_2})$ are combined to determine the impact force generated on both masses at the time of the collision and can be written as,

$$F_c = k_{eq} H(x_1, x_2) + c_{eq} G(\dot{x}_1, \dot{x}_2)$$
(11)

The natural frequency of primary mass and particle upon impact can be adjusted by choosing an appropriate material for the impact surface with the necessary stiffness (k_{eq}). The natural frequencies of both masses are then calculated as follows:

$$\omega_1 = \sqrt{k_1/M}$$
, $\omega_2 = \sqrt{k_{eq}/m}$

While the frequency ratio is defined as,

$$\gamma = \frac{\omega_2}{\omega_1} = \frac{\sqrt{k_{eq}/m}}{\sqrt{k_1/M}} \tag{12}$$

A relative clearance magnitude is used in the analysis for generalization purposes. The relative clearance magnitude is defined as,

$$D = \frac{d}{Y} \tag{13}$$

Here *Y* is the amplitude of ground motion. Given the linear contact model illustrated in figure 2(b), if the impact surface is softer, it can be depicted as an equivalent spring and damper system. The equation of motion

for both masses while in contact can be formulated as follows:

$$M\ddot{x}_1 + k_{eq}(x_1 - x_2) + c_{eq}(\dot{x}_1 - \dot{x}_2) = 0$$
(14)

$$m\ddot{x}_2 + k_{eq}(x_2 - x_1) + c_{eq}(\dot{x}_2 - \dot{x}_1) = 0$$
(15)

$$If z = x_1 - x_2,$$

$$M\ddot{x}_1 + k_{eq}z + c_{eq}\dot{z} = 0 {16}$$

$$m\ddot{x}_2 - k_{eq}z - c_{eq}\dot{z} = 0 ag{17}$$

Multiplying equation (17) with M/m,

$$M\ddot{x}_2 - k_{eq} \frac{M}{m} z - c_{eq} \frac{M}{m} \dot{z} = 0$$
 (18)

Subtracting equation (18) from 16 gives,

$$M\ddot{z} + k_{eq}z + \frac{k_{eq}M}{m}z + c_{eq}\dot{z} + \frac{c_{eq}M}{m}\dot{z} = 0$$
 (19)

$$M\ddot{z} + k_{eq} \left(1 + \frac{M}{m}\right) z + c_{eq} \left(1 + \frac{M}{m}\right) \dot{z} = 0$$
 (20)

If the motion is harmonic, it can be assumed that,

$$x_1(t) = Ae^{-\zeta\omega_n t}\sin(\omega_d t + B) \tag{21}$$

Here $\omega_d = \omega_n \sqrt{1-\zeta^2}$ is the damped natural frequency. To determine the damping resulting from impact, the logarithmic decrement method can be used by analyzing the velocity response of the system. Assuming that there are two collisions per cycle, the half logarithmic decrement approach can be employed to assess the damping from a single impact.

$$\delta = \ln\left(\frac{\dot{x}_1^+}{\dot{x}_1^-}\right) = 2\ln e \tag{22}$$

$$\zeta_{eq} = -\frac{\ln e}{\sqrt{\pi^2 + (\ln e)^2}} \tag{23}$$

From equation (20), $\omega_n = \sqrt{\frac{k_{eq}(m+M)}{(mM)}}$ and $\zeta_{eq} = \frac{c_{eq}\left(1+\frac{M}{m}\right)}{2\sqrt{Mk_{eq}\left(1+\frac{M}{m}\right)}}$ are the natural frequency and equivalent

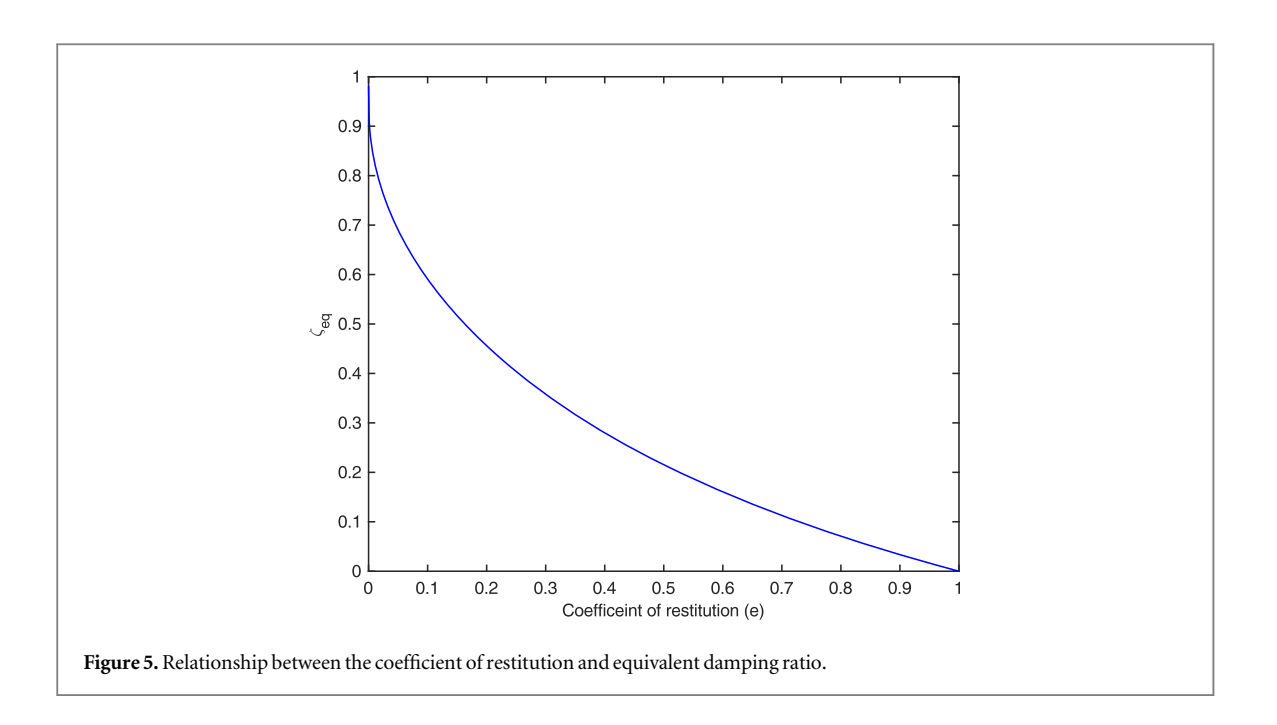
damping ratio of the system. Rearranging the expression of damping ratio for equivalent damping coefficient,

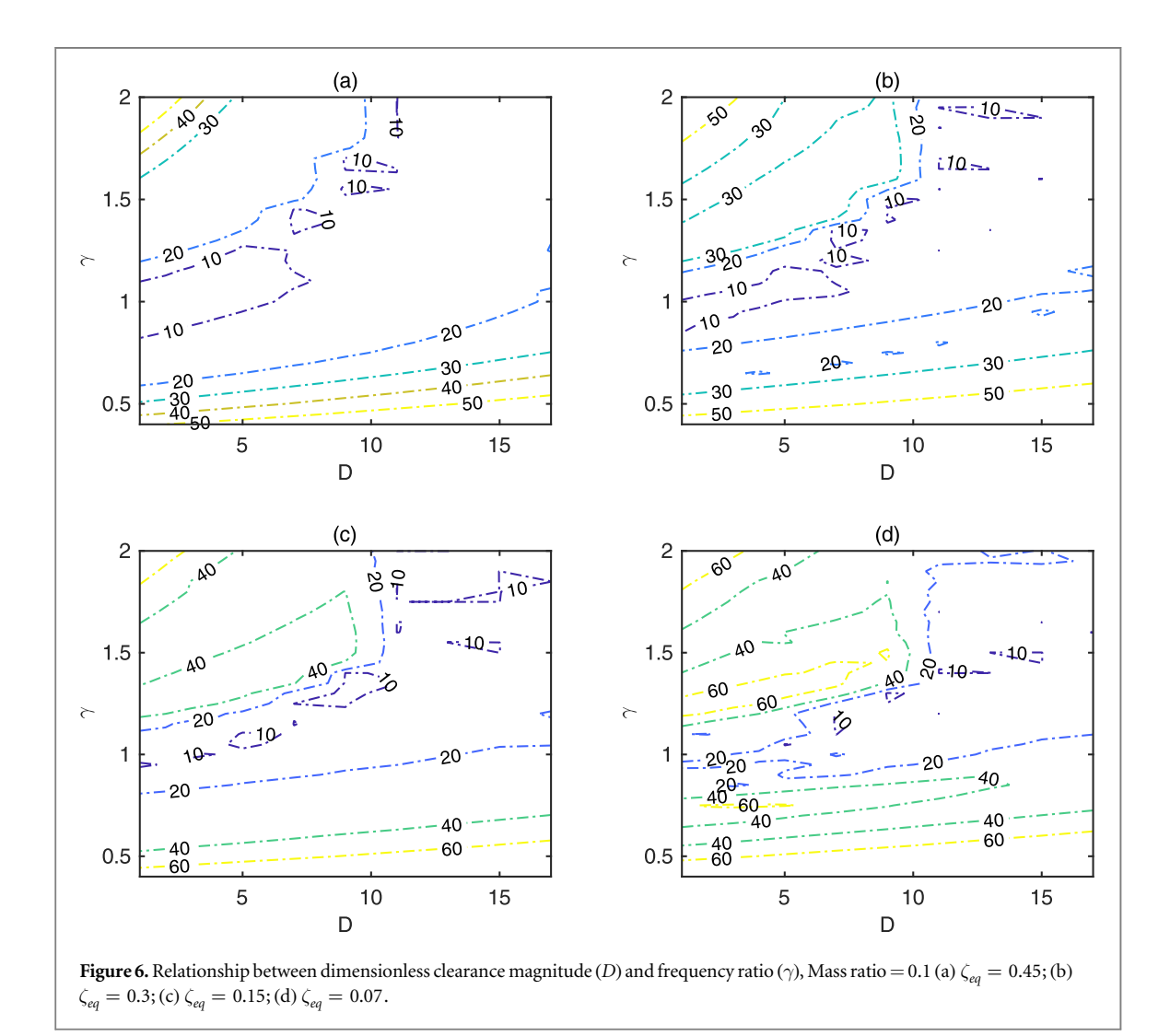
$$c_{eq} = 2\zeta_{eq} \sqrt{k_{eq} \frac{mM}{m+M}} \tag{24}$$

When employing a soft impact surface, it is expected that energy dissipation will occur during the collision. This impact model effectively includes this phenomenon by introducing an equivalent viscous damping coefficient. The energy dissipation during the collision can be derived from the coefficient of restitution specific to the material. Equations (22) and (23) can be used to calculate the equivalent viscous damping coefficient for any given impact surface. The relationship between the coefficient of restitution and the equivalent damping ratio of any impact surface is illustrated in figure 5.

As previously mentioned, TMD must be tuned to a specific frequency ratio (γ), ensuring that the secondary mass's natural frequency closely aligns with that of the host structure, while precise damping ratios are crucial for optimal energy dissipation. Deviating from the required damping ratio range may result in detuning of the TMD system. In contrast, the secondary mass in SPID is not continuously linked to the host structure; instead, direct connections occur intermittently, altering the system dynamics over time. Unlike TMD, SPID introduces an additional design parameter known as dimensionless clearance magnitude (D). Various researchers have highlighted the significance of clearance as a fundamental design parameter in particle damping. Consequently, this study delves into the examination of clearance magnitude alongside other design parameters. The clearance magnitude D is defined as the ratio of the clearance distance (d) to the amplitude of the base excitation (Y), facilitating the generalization of results.

Figure 6 illustrates contour plots describing the dynamic vibration amplitude (X/Y) across various combinations of frequency ratio (γ) and clearance magnitude (D) for randomly chosen damping ratios ζ_{eq} . The results indicate that a frequency ratio close to 1 yield better vibration suppression, as mutual resonance enhances energy transfer and dissipation. However, the results demonstrate that comparable damping performance can be attained across a range of damping ratios, addressing the concerns associated with TMD. Although the vibration amplitude may not reach the minimal levels observed with TMD, a satisfactory level of damping can





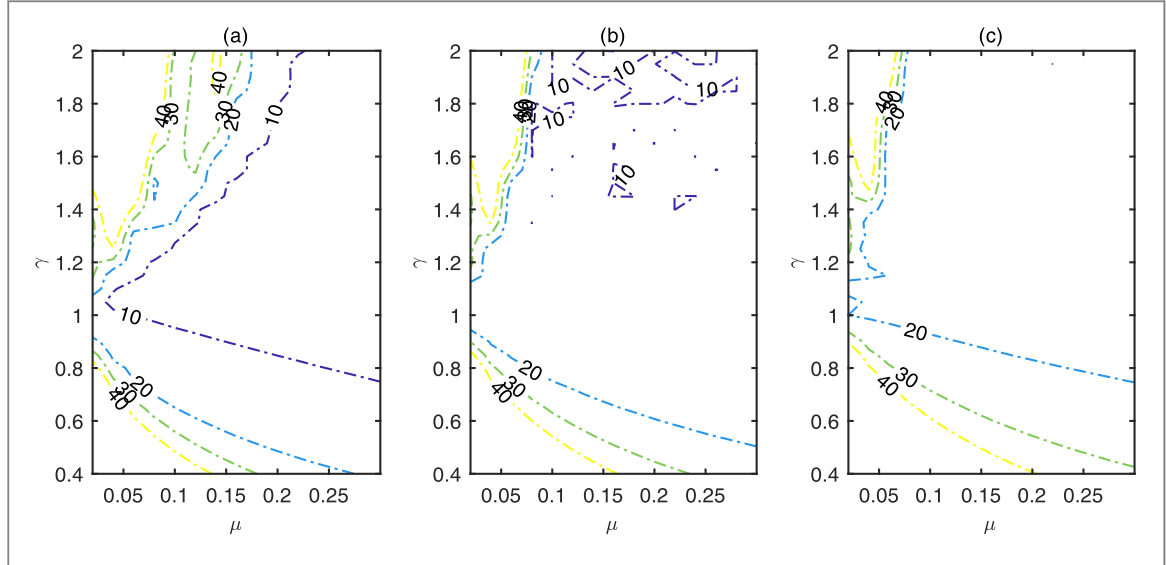


Figure 7. Variation of vibration amplitude over various combinations of mass ratio and frequency ratio. $\zeta_{eq}=0.45$, (a) D=5; (a) D=10; (a) D=15. D represents the dimensionless clearance magnitude.

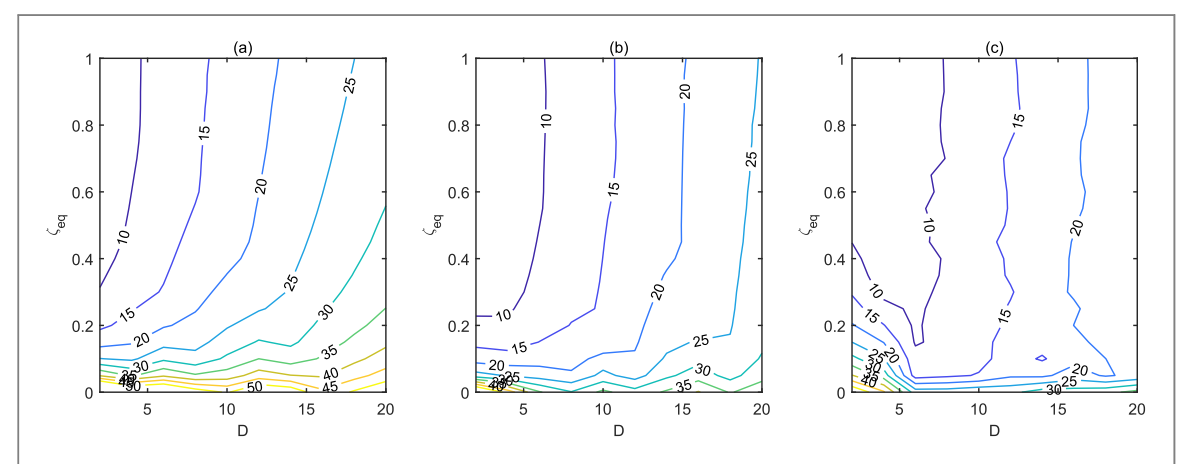


Figure 8. Contour of dynamic vibration amplitude over different combinations of dimensionless clearance magnitude (D) and equivalent damping ratio (ζ_{ea}); (a) $\gamma = 0.9$; (b) $\gamma = 1.0$; (c) $\gamma = 1.1$. γ represents the frequency ratio.

still be achieved through a simple design and installation process. Consequently, designers can select a design tailored to their specific application requirements based on the guidelines outlined in this study.

The contour plots shown in figure 7 demonstrate the impact of particle mass on the frequency ratio across various clearance magnitudes, while keeping ζ_{eq} constant. From figure 7(a), it is evident that damping performance relies on both the mass ratio and γ concurrently, particularly noticeable when the clearance magnitude is smaller (i.e., D=5). Substantial vibration suppression can be attained with a lesser particle mass (approximately 5%) when γ approaches 1. However, as the mass ratio increases, the impact of γ begins to diminish. Conversely, as illustrated in figures 7(b) and (c), the influence of γ significantly decreases with increased clearance. These graphs illustrate that an amplitude ratio within 10 can be achieved across various combinations of mass ratio and γ , particularly with a clearance magnitude around 10. These results underscore the paramount importance of clearance magnitude as the most influential parameter in particle damping.

In contrast, figure 8 displays contour plots of vibration amplitude across various combinations of dimensionless clearance magnitude and damping ratio, with the frequency ratio held constant. It is evident that the damping performance of the SPID is dependent on the dimensionless clearance magnitude (D). As the clearance gap increases, the influence of the damping ratio becomes minimal; however, it appears that a very low damping ratio $\zeta_{eq} < 0.2$ may detrimentally impact the overall damping performance. In summary, the proposed SPID demonstrates notable efficiency in vibration control, offering a simple design and installation

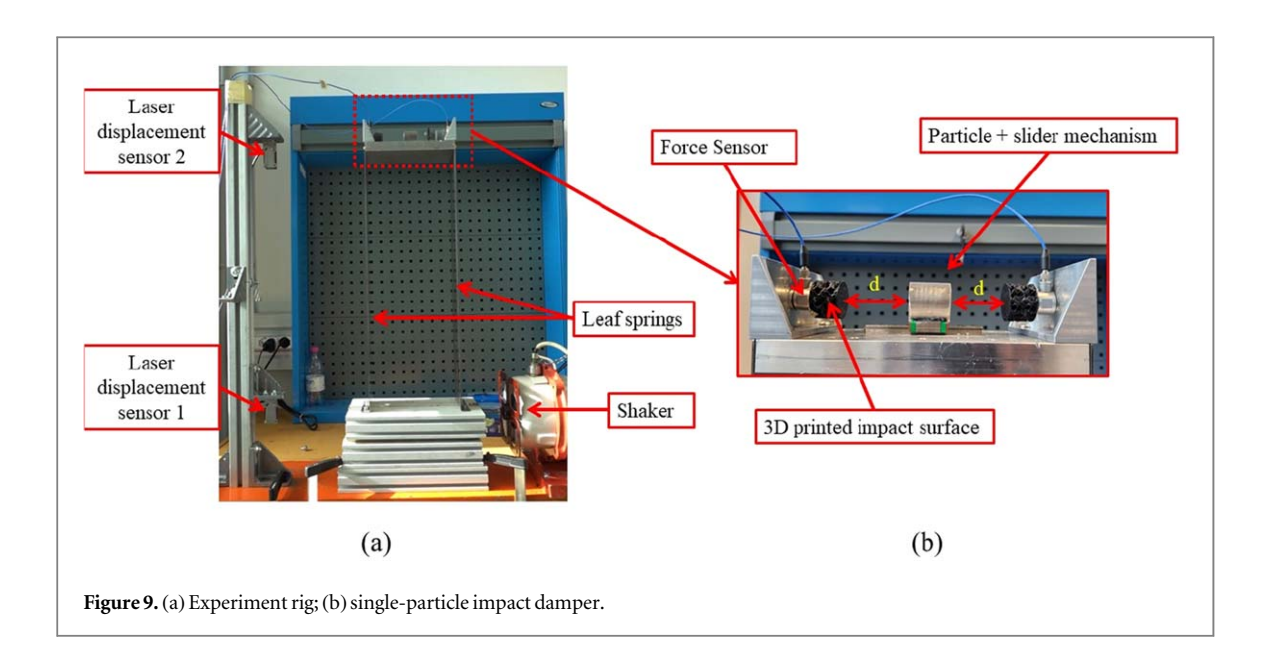


Table 1. Parameters of the host structure.

| Parameter | Magnitude | | |
|--------------------------------|-----------|--|--|
| Mass (M) | 1.6 Kg | | |
| Natural frequency (ω_n) | 2.5 Hz | | |
| Structural damping | 0.0038 | | |

process. While the damping rate provided by the SPID may not match that of traditional TMD systems, it still delivers substantial damping across various design configurations.

To address the limitations of the Linear Contact Model (LCM) in capturing key physical phenomena, we acknowledge the importance of considering nonlinear contact dynamics. A Hertzian-type nonlinear stiffness model for elastic impacts, combined with restitution or plastic deformation effects dependent on velocity, could provide a more comprehensive representation of particle-wall interactions. For instance, the Hertzian contact model incorporates the relationship between contact force and deformation, which is particularly relevant for softer materials or higher impact velocities. While the LCM simplifies the analysis by assuming linear stiffness and neglecting energy dissipation during collisions, it may not accurately capture the behavior of materials with significant viscoelastic damping or plastic deformation. Future work could explore nonlinear contact models, such as the Hertzian model with viscoelastic damping, to evaluate their accuracy across different impact regimes and compare their performance with the LCM. This would help identify the limitations of the LCM and determine its applicability for specific material properties and impact conditions.

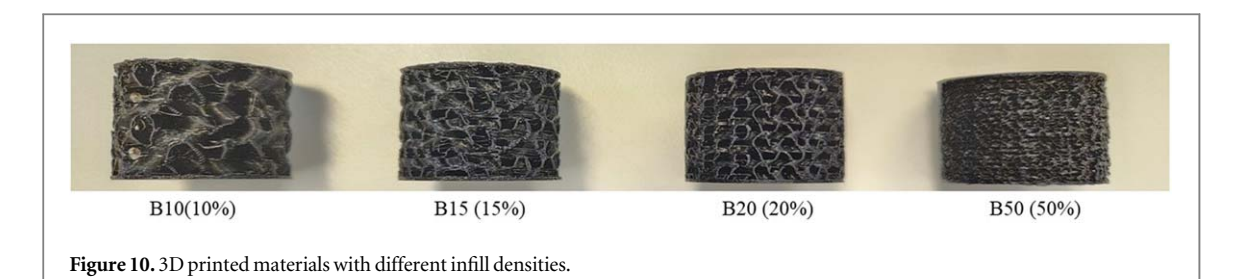
3. Experiments

This section provides the details about the experiment setup. This includes the details of the primary structure, sensors used and their placements with an overall procedure leading to the experimental results.

3.1. Experimental setup

A single-degree-of-freedom structure is assembled, consisting of two steel beams acting as leaf springs with an aluminum block serving as the primary mass affixed at the top, as illustrated in figure 8. A moveable base connected to a shaker is employed to provide the base excitations for the primary mass. Additionally, two non-contact laser displacement sensors are positioned to record the displacement of both the primary mass (at the top) and the base (at the bottom) as shown in figure 9(a).

Free vibration tests are conducted to determine the dynamic characteristics of the primary mass. The parameters of the primary mass are presented in table 1. The damping ratio is obtained by employing the logarithmic decrement method on the free vibration response of the primary mass.



Moreover, a SPID (as depicted in figure 8(b)) features a sliding mechanism, offering two significant advantages: (1) it ensures unidirectional movement for the particle and (2) minimizes friction. Two Dytran 1051-V2 force sensors are included between the walls of the SPID and the 3D printed materials. These force sensors are employed to capture the impact force transmitted to the primary structure via various impact surfaces. The clearance (denoted as 'd' in figure 9(b)) between the particle and the walls of the primary structure can be adjusted by displacing the L-beams located at either end. The prototype of the single-particle impact damper, as shown in figure 9(b), can adapt total clearance lengths (2d) of 30 mm, 60 mm, and 90 mm, respectively.

3.2. Dynamic tests on 3D printed materials

The experimental validations aim to demonstrate that the SPID can maintain consistent damping performance across various design parameter ranges. To achieve this, materials are 3D printed with varying infill densities, as illustrated in figure 10. The experimental validation of the SPID is conducted using 3D-printed materials with varying mechanical properties, including stiffness and damping coefficients. The infill density of the printed materials dictates dynamic properties like stiffness and damping coefficients. All printed materials are standardized at 30 mm diameter and 20 mm height. Additionally, Ninja Flex 85A, a thermoplastic polyurethane (TPU) material is utilized for 3D prototyping. It has a shore hardness of 85A, Tensile modulus of 12 Mpa, and ultimate tensile strength of 26 Mpa. Several factors, including printing temperature, printing speed, and infill density, can influence the final print properties. To maintain consistency, these parameters are strictly kept consistent while printing the two 3D models for each side of the SPID.

The dynamic analysis requires experimental determination of properties such as stiffness and damping ratio for the printed materials. To achieve this, the frequency response spectrum is measured for each printed material using an impact hammer model test, a conventional method in dynamic testing. Specifically, an impact hammer model PCB 086C01, having a sensitivity of $11.2 \, \text{mV N}^{-1}$, is employed to control the force. Meanwhile, an accelerometer (PCB 352A24) is attached to the mass to capture the structural acceleration response under the applied force, as illustrated in figure 9.

Data acquisition from both the force sensor attached to the impact hammer and the accelerometer is facilitated through a LabView software program. Subsequently, the acquired data is processed to ascertain the Frequency Response Function (FRF). The mass attached to the printed materials is of a 165-gram cylinder. Subsequently, this cylinder is reused as the particle within the SPID setup. The Frequency Response Function (FRF) data obtained from the dynamic tests allows the extraction of stiffness and damping coefficients for each printed material. The natural frequency associated with each material is identified from the FRF curve, shown in figure 11. The stiffness is then computed using the following equation:

$$2\pi f_n = \sqrt{\frac{k}{M}} \tag{25}$$

Using equation 25, the stiffness of each printed material can be calculated as presented in table 2. Additionally, the damping coefficient of each printed material is determined from the damping ratio calculated from the FRF curve using the 3 dB method.

4. Results and discussion

Once all dynamic properties of the impact surface materials and primary mass are determined, experiments commence by subjecting the primary structure to sinusoidal base excitation. Notably, conventional sweep-sine tests prove inadequate for assessing SPID due to potentially prolonged transient periods. Consequently, the primary structure's steady-state response is recorded within a narrow frequency range surrounding its natural frequency. Subsequently, the steady-state response amplitudes across this range are aggregated and plotted

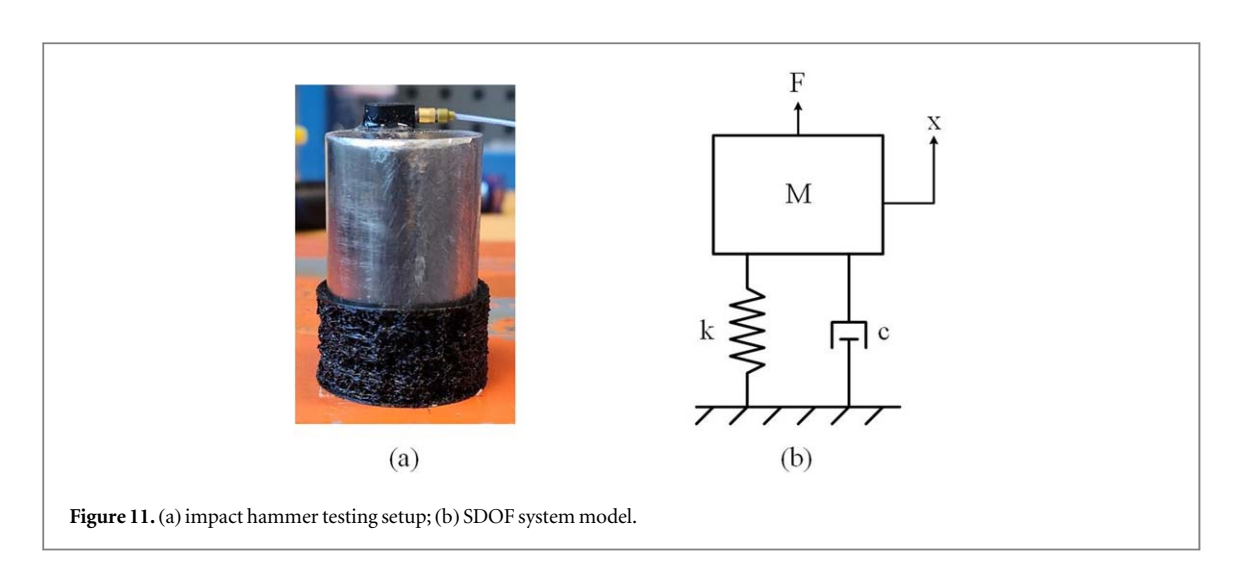


Table 2. The properties of the printed materials from dynamic test.

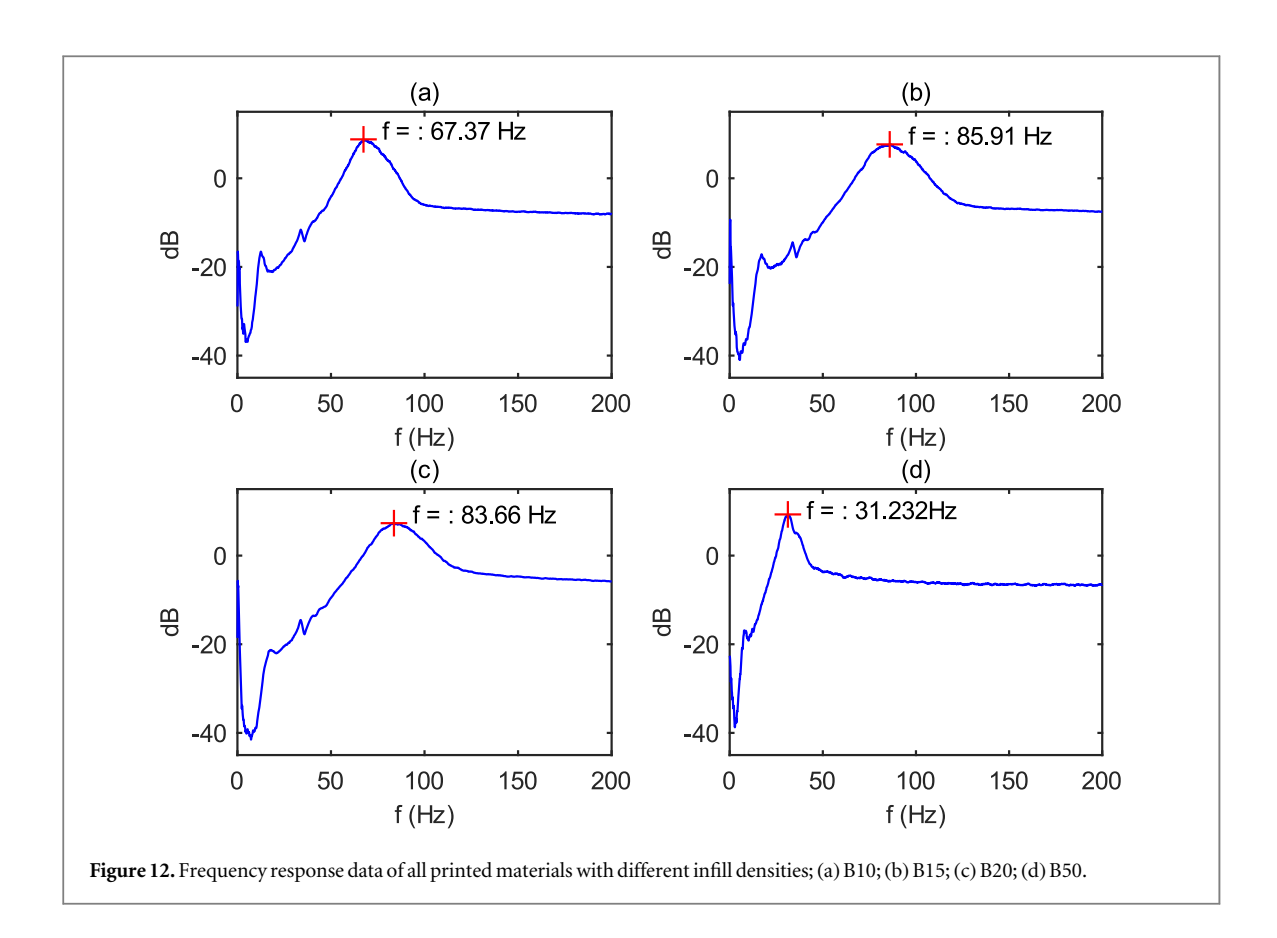
| Impact surface | Stiffness (k) kN/m | Damping coefficient (c) Ns/m | | |
|----------------|-----------------------|------------------------------|--|--|
| | Ki t/ III | 110/111 | | |
| B10 | 29.57 | 14.54 | | |
| B15 | 48.08 | 23.88 | | |
| B20 | 45.59 | 23.35 | | |
| B50 | 6.35 | 5.62 | | |

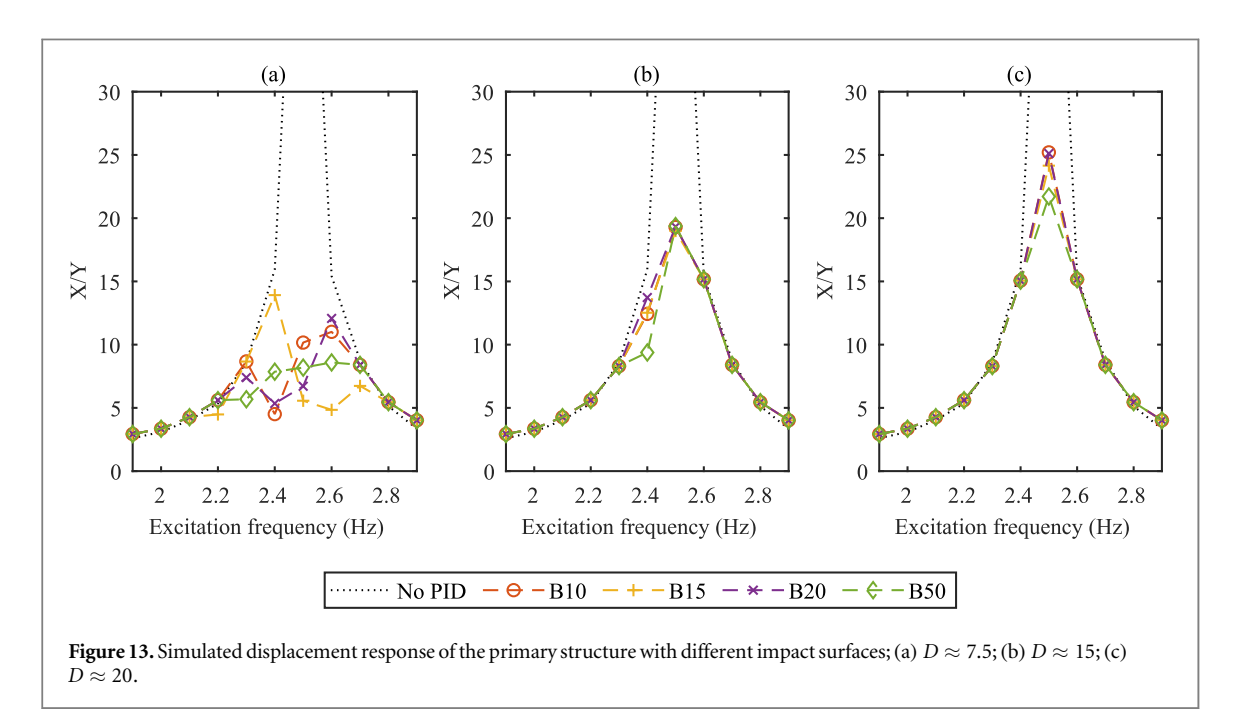
against the excitation frequencies, producing the frequency response of the primary structure with varying impact surfaces. The ratio of the particle mass to the host structure is a critical parameter influencing the performance of the SPID. While the current study focuses on a fixed mass ratio (μ = 0.1). Although varying this ratio could significantly affect energy dissipation leading to superior damping performance similar to TMD system. For instance, a higher mass ratio may enhance energy transfer during collisions, potentially improving damping performance. However, it could also increase the complexity of the system dynamics and affect the overall stability of the host structure. Additional mass is generally very limited in practical application such as high-rise structure may allow a 1%–2% mass for a damper, machinery or aerospace applications may allow up to 10%–15% additional mass. Therefore, a fixed mass ratio of 10% is used in this study for simplicity of analysis and results. Additionally, experimental parameters are integrated into the numerical model, and the corresponding numerical outcomes are illustrated in figure 12.

The numerical findings reveal that the single-particle impact damper can be configured across various parameter combinations. To substantiate these conclusions, the numerical results are cross-referenced with experimental data. Figures 13 and 14 illustrate the frequency response of the primary structure under different parameter settings from simulations and experiments, respectively. A comparison between the simulated outcomes (figure 13) and the experimental findings (figure 14) underscores the alignment between the numerical model and experimental observations.

The comparative analysis of maximum vibration amplitudes obtained from numerical simulations and experimental data for various impact surfaces and clearance magnitudes is depicted in table 3. The data in table 3 compares the numerical simulation results with experimental test data for the vibration amplitude reduction achieved by the SPID using different materials (B10, B15, B20, B50) and clearance magnitudes (D \approx 7.5, D \approx 15, D \approx 20). The simulations generally align with the experimental results, showing a reduction in vibration amplitude as the clearance increases. There are slight differences in the results observed as well, and these differences may arise from factors such as material property variations, experimental uncertainties, or simplifications in the numerical model. The general trend, however, indicates that increasing clearance effectively reduces vibration amplitude, supporting the design premise of the SPID.

The linear contact model simplifies the analysis by neglecting nonlinear effects such as restitution and plastic deformation, which may reduce accuracy in certain scenarios. However, the model provides a practical and computationally efficient framework for SPID design. Future research could explore nonlinear models to evaluate their impact on vibration reduction effectiveness. The study primarily focuses on the behavior of the Single-Particle Impact Damper (SPID) near resonance, where damping performance is most critical. However, it is acknowledged that SPIDs may exhibit chaotic behavior under certain conditions, particularly in higher





modes or during broadband excitation. However, previous studies have shown that the chaotic behaviour can be controlled with the proper selection of parameters such as mass ratio and clearance magnitude (Akbar *et al* 2024a, 2024b). In this study, the selected parameters are within the range of nonchaotic behaviour and there were no observations of such behaviour from numerical and experimental results. On the other hand, future research could include a study of non-resonant excitation or transient response, such as impulse or broadband input, to better understand the system's behavior outside the resonance regime.

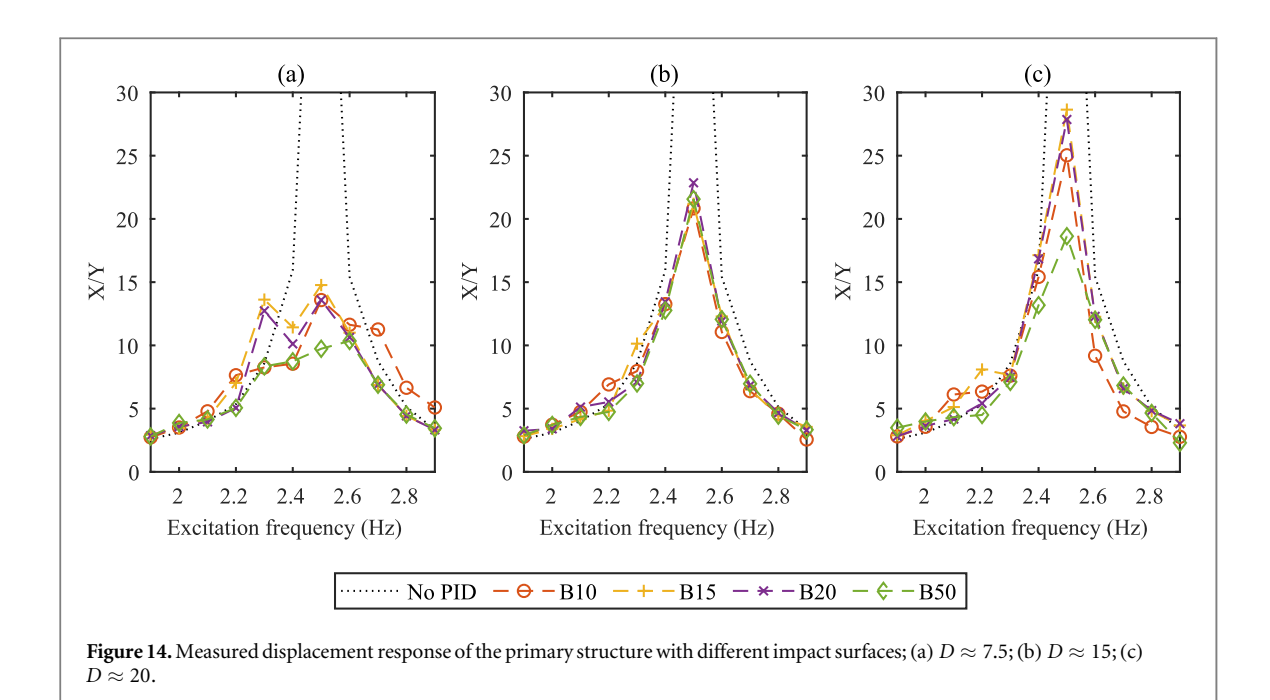


Table 3. Comparison of maximum vibration amplitude from simulations and experiments

with different impact surfaces and clearance size.

| | X/Y | | | | | | |
|-----|---------------|-------|---------------|-------|------------|-------|--|
| | <i>D</i> ≈7.5 | | <i>D</i> ≈ 15 | | D≈20 | | |
| | Simulation | Test | Simulation | Test | Simulation | Test | |
| B10 | 11.01 | 13.58 | 19.29 | 20.82 | 25.20 | 25.02 | |
| B15 | 14.24 | 15.00 | 19.24 | 21.47 | 22.47 | 26.65 | |
| B20 | 11.08 | 13.61 | 20.31 | 24.02 | 24.51 | 27.20 | |
| B50 | 8.34 | 9.68 | 20.03 | 22.29 | 23.61 | 20.26 | |

5. Conclusions

This research investigates the functionality of a single-particle impact damper (SPID) utilizing a linear contact model to simulate collision dynamics, with experimental validation. The study aims to demonstrate the SPID as a viable alternative to traditional tuned mass dampers (TMD) for mitigating resonance peaks. The complex nature of TMD design parameters and the inherent detuning challenges have been extensively highlighted by researchers, leading to increased complexity, installation difficulties, and higher costs. In contrast, the SPID offers comparable performance to TMD across a wider range of design parameters.

In TMD design, meticulous selection and calibration of the damping constant are crucial for optimal functionality, as even small adjustments can have significant effects on system performance. In contrast, numerical analysis of the SPID reveals that varying combinations of design parameters, particularly different damping coefficients, can achieve comparable damping performance. Furthermore, the clearance magnitude in impact dampers is identified as a critical factor influencing damping performance. Proper selection of clearance magnitude significantly enhances the SPID's damping capabilities, regardless of other design parameters.

While the SPID may not match the damping performance of an optimized TMD, it demonstrates noticeable reductions in vibration amplitude at resonance. To validate the numerical findings, an experimental setup consisting of a frame structure and the SPID is constructed. Various stoppers with different mechanical properties are 3D printed to validate the results, and mechanical properties are evaluated using Frequency Response Function (FRF) tests. Both experimental and numerical results confirm the SPID's ability to deliver reliable damping across diverse parameter combinations.

While the linear contact model provides a simplified yet effective framework for SPID design, it assumes negligible energy dissipation during collisions, which may not hold true for all materials or impact conditions. Future work could explore nonlinear contact models to improve the accuracy of predictions, especially for softer or more compliant materials. Overall, the SPID stands out as a cost-effective option for various vibration control

applications, thanks to its straightforward design and installation methods. Its broader range of design parameter combinations and comparable performance to TMD make it an appealing choice for mitigating resonance peaks. Engineers could benefit from the results from this study such as the design parameters of SPID for designing the damper for several applications. Further research and development in this area can contribute to expanding the applications of the SPID and enhancing its damping performance in real-world engineering scenarios.

Data availability statement

All data that support the findings of this study are included within the article (and any supplementary files).

ORCID iDs

Muhammad Ayaz Akbar https://orcid.org/0000-0002-2038-6823 Hassan Raza https://orcid.org/0000-0001-8672-7865

References

Afsharfard A and Farshidianfar A 2011 An efficient method to solve the strongly coupled nonlinear differential equations of impact dampers Arch. Appl. Mech. 82 977–84

Akbar M A, Wong W O and Rustighi E 2023 A hybrid damper with tunable particle impact damping and coulomb friction *Machines* 11 545 Akbar M A, Wong W and Rustighi E 2024a A study of soft and hard impact effects in single-particle impact dampers *J. Vib. Control* 0 10775463241273063

Akbar M A, Wong W O and Rustighi E 2024b Design optimization of a single-mass impact damper *J. Sound Vib.* **570** 118019

Badri Y, Sassi S, Hussein M and Renno J 2021 Experimental and numerical investigation of damping in a hybrid automotive damper combining viscous and multiple-impact mechanisms *J. Vib. Control* **28** 3676–87

Bryce L F, Eric M F and Steven E O 2001 Design methodology for particle damping Smart Structures and Materials: Damping and Isolation SPIE 4331 186–97

Chan K W, Liao W H, Wang M Y and Choy P K 2016 Experimental studies for particle damping on a bond arm *J. Vib. Control* 12 297–312 Chen J and Georgakis C T 2013 Tuned rolling-ball dampers for vibration control in wind turbines *J. Sound Vib.* 332 5271–82

Chen J L, Wang Y C, Zhao Y and Feng Y Q 2019 Experimental research on design parameters of basin tuned and particle damper for wind turbine tower on shaker Structural Control & Health Monitoring 26 e2440

Duvigneau F, Koch S, Woschke E and Gabbert U 2016 An effective vibration reduction concept for automotive applications based on granular-filled cavities *J. Vib. Control* 24 73–82

Ekwaro-Osire S and Desen I C 2016 Experimental study on an impact vibration absorber J. Vib. Control 7 475–93

Fadel Miguel L F, Lopez R H, Miguel L F F and Torii A J 2016 A novel approach to the optimum design of MTMDs under seismic excitations Structural Control and Health Monitoring 23 1290–313

Friend R D and Kinra V K 2000 Particle impact damping J. Sound Vib. 233 93-118

Gagnon L, Morandini M and Ghiringhelli G L 2019 A review of particle damping modeling and testing J. Sound Vib. 459 114865

Gardonio P and Elliott S J 2000 Passive and active isolation of structural vibration transmission between two plates connected by a set of mounts J. Sound Vib. 237 483–511

Gourc E, Seguy S, Michon G, Berlioz A and Mann B P 2015 Quenching chatter instability in turning process with a vibro-impact nonlinear energy sink *J. Sound Vib.* 355 392–406

Guo X, Zhu Y and Cao D 2025 Dynamic design and performance prediction of tuned particle dampers based on co-simulation Nonlinear Dyn. 113 3053–77

Guo Y, Liu K and Hou G 2024 Experimental study on damping characteristics of the particle dampers with damping rod and soft inside wall J. Phys. Conf. Ser. 2704 012025

Hartog D J 1956 Mechanical Vibrations (McGraw-Hill Book Company)

Hastie D B 2013 Experimental measurement of the coefficient of restitution of irregular shaped particles impacting on horizontal surfaces Chem. Eng. Sci. 101 828–36

Hu L, Shi Y G, Yang Q L and Song G B 2016 Sound reduction at a target point inside an enclosed cavity using particle dampers *J. Sound Vib.* 384 45–55

Huang X H, Li X J and Wang J 2021 Optimal design of inerter-based nonpacked particle damper considering particle rolling Earthq. Eng. Struct. Dyn. 50 1908–30

Jadhav T A and Awasare P J 2016 Enhancement of particle damping effectiveness using multiple cell enclosure *J. Vib. Control* 22 1516–25 Jin G, Zhao Z H, Liu B B, Cun W Y, Zhao Z D, Hou M L and Chen G 2021 Design of a particle damper and experimental study on vibration damping of the pipeline *Advances in Mechanical Engineering* 13 168781402110449

Jin J, Sun X, Liu Y and Chen Z 2024 Research on active-passive integrated vibration isolator based on metal rubber and piezoelectric actuator Smart Mater. Struct. 33 095036

Kumar S and Kumar A 2024 Vibration attenuation of a PCB enclosure in a radar system employing internal particle dampers *Int. J. Mech. Mater. Des.* 21 137–53

Li K and Darby A P 2016 Experiments on the effect of an impact damper on a multiple-degree-of-freedom system *J. Vib. Control* 12 445–64 Li X, Yang, Y, Shi, W and Caterino N 2019 Study on the damping effect of particle dampers considering different surface properties *Shock and Vibration* 2019 1–16

Liu W, Tomlinson G and Worden K 2002 Nonlinearity study of particle dampers Int. Conf. on Noise and Vibration Engineering (ISMA2002). Katholieke Univ Leuven, Dept Werktuigkunde 495–9

Lu Z, Zhang J and Wang D 2021 Energy analysis of particle tuned mass damper systems with applications to MDOF structures under wind-induced excitation J. Wind Eng. Ind. Aerodyn. 218 104766

Marhadi K S and Kinra V K 2005 Particle impact damping: effect of mass ratio, material, and shape J. Sound Vib. 283 433–48 Masri S F 1970 General motion of impact dampers J. Acoust. Soc. Am. 47 229–37

Michael Y Y, George A L, Stephen A H and Gary H K 2004 Development of a design curve for particle impact dampers *Noise Control Eng. J.* 53 5–13

Papalou A and Masri S F 2016 An experimental investigation of particle dampers under harmonic excitation *J. Vib. Control* 4 361–79
Patil K A, Katake K A, Sutar K B and Karande P S 2025 Experimental investigation on suppression of gearbox vibrations using particle damping technique *Engineering Research Express* 7 015568

Popplewell N and Liao M 1991 A simple design procedure for optimum impact dampers J. Sound Vib. 146 519-26

Prasad B B, Duvigneau F, Juhre D and Woschke E 2022 Damping performance of particle dampers with different granular materials and their mixtures *Appl. Acoust.* 200 109059

Prasad B B, Duvigneau F, Woschke E and Juhre D 2023 Application and damping mechanism of particle dampers *PAMM* 22 Sánchez M, Carlevaro C M and Pugnaloni L A 2013 Effect of particle shape and fragmentation on the response of particle dampers *J. Vib. Control* 20 1846–54

Sánchez M and Manuel Carlevaro C 2013 Nonlinear dynamic analysis of an optimal particle damper *J. Sound Vib.* 332 2070–80 Snoun C and Trigui M 2018 Design parameters optimization of a particles impact damper *International Journal on Interactive Design and Manufacturing (IJIDeM)* 12 1283–97

Song C, Han Y, Jia B, Xiong X, Jiang Y, Wang P, Liang Y and Fang H 2024 Analysis of vibration reduction performance of vibration isolation system based on particle damping *Journal of Low Frequency Noise*, Vibration and Active Control 43 1244–60

Tran V-Q, Wu Y-R and Ke N-Y 2025 An experimental study on rotor dynamic balancing and structural vibration attenuation for a motor reducer with damping particles *Journal of Vibration Engineering & Technologies* 13 317

Veeramuthuvel P, Sairajan K K and Shankar K 2016 Vibration suppression of printed circuit boards using an external particle damper J. Sound Vib. 366 98–116

Wang Q and Dan D 2022 A simplified modeling method for multi-particle damper: validation and application in energy dissipation analysis J. Sound Vib. 517 116528

Wong C and Rongong J 2009 Control of particle damper nonlinearity AIAA J. 47 953–60

Wong CX, Daniel MC and Rongong JA 2009 Energy dissipation prediction of particle dampers J. Sound Vib. 319 91-118

Wong W O 2016 Optimal design of a hysteretic vibration absorber using fixed-points theory *J. Acoust. Soc. Am.* 139 3110–5

Wong W O, RP F and Cheng F 2018 Design optimization of a viscoelastic dynamic vibration absorber using a modified fixed-points theory J. Acoust. Soc. Am. 143 1064–75

Xu Z W, Chan K W and Liao W H 2004 An empirical method for particle damping design Shock and Vibration 11 647-64

Yang F, Sedaghati R and Esmailzadeh E 2021 Vibration suppression of structures using tuned mass damper technology: a state-of-the-art review J. Vib. Control 28 812–36

Yang Y Q and Wang X 2019 Investigation into the linear velocity response of cantilever beam embedded with impact damper *J. Vib. Control* 25 1365–78

 $Zhang J, Zhu Y, Tu J, Li Z \ and \ Wang Q \ 2022 \ Development \ and \ vibration \ control \ of \ frequency \ adjustable \ tuned \ mass \ damper \ based \ on \ magnetorheological \ elastomer \ \textit{Materials} \ 15 \ 1829$

 $Zhao\ Z, Zhang\ R\ and\ Lu\ Z\ 2019\ A\ particle\ inerter\ system\ for\ structural\ seismic\ response\ mitigation\ \emph{\emph{J. Franklin Inst.}}\ 356\ 7669-88$

Zhou S, Lu F, Wu Z, Zhang C, Mo W and Zhu Y 2025 Theoretical and simulation study of active vibration control of Miura-ori core sandwich beam *Smart Mater. Struct.* 34 045012

Zilletti M, Elliott S J and Rustighi E 2012 Optimisation of dynamic vibration absorbers to minimise kinetic energy and maximise internal power dissipation *J. Sound Vib.* 331 4093–100